

# Activatable Singlet Oxygen Generation from Lipid Hydroperoxide Nanoparticles for Cancer Therapy

Zijian Zhou<sup>†</sup>, Jibin Song<sup>†</sup>, Rui Tian, Zhen Yang, Guocan Yu, Lisen Lin, Guofeng Zhang, Wenpei Fan, Fuwu Zhang, Gang Niu, Liming Nie,<sup>\*</sup> and Xiaoyuan Chen<sup>\*</sup>

**Abstract:** Reactive oxygen species (ROS)-induced apoptosis is a widely practiced strategy for cancer therapy. Although photodynamic therapy (PDT) takes advantage of the spatial-temporal control of ROS generation, the meticulous participation of light, photosensitizer, and oxygen greatly hinders the broad application of PDT as a first-line cancer treatment option. An activatable system has been developed that enables tumor-specific singlet oxygen ( $^1O_2$ ) generation for cancer therapy, based on a Fenton-like reaction between linoleic acid hydroperoxide (LAHP) tethered on iron oxide nanoparticles (IO NPs) and the released iron(II) ions from IO NPs under acidic-pH condition. The IO-LAHP NPs are able to induce efficient apoptotic cancer cell death both *in vitro* and *in vivo* through tumor-specific  $^1O_2$  generation and subsequent ROS mediated mechanism. This study demonstrates the effectiveness of modulating biochemical reactions as a ROS source to exert cancer death.

Reactive oxygen species (ROS) serve as a double-edged sword in the cell life cycle, functioning as an important messenger during cell proliferation and homeostasis at low level.<sup>[1]</sup> Whereas breaking the threshold of ROS level would lead to oxidative damage to cellular constituents and then apoptotic or necrotic cell death.<sup>[2]</sup> Photodynamic therapy (PDT) is among the most widely considered strategies for ROS-mediated cancer treatment by photodynamic effect between light source, photosensitizer, and oxygen.<sup>[3]</sup> After several generations of PDT drugs have been developed, however, PDT still have not gained acceptance as a first-line treatment option. This can be largely attributed to the fact that several major challenges of traditional PDT remain unresolved at different levels, such as limited light penetra-

tion depth, oxygen reliance, and systemic toxicity derived from off-site localization and self-catalysis of photosensitizers.<sup>[3a,4]</sup> Advances in nanotechnology and nanomedicine have spurred numerous designing considerations to meet these critical challenges.<sup>[5]</sup> For examples, the use of nanoscintillators as light transducers to improve the light penetration depth,<sup>[6]</sup> and the oxygen self-supplied systems to tackle the situation of oxygen insufficiency.<sup>[7]</sup> It is worth noting that these procedures still rely on photosensitization effect during which the meticulous cooperation between light, photosensitizer, and oxygen may render the treatment outcomes with respectable complexity and variability.<sup>[8]</sup>

In essence, ROS, as an important chemical substrate, has been extensively studied through methods other than photosensitization.<sup>[9]</sup> During aerobic respiration, oxygen is reduced along the electron transport chains in mitochondria, which leads to the formation of ROS byproducts throughout the cell lifetime.<sup>[10]</sup> The failure to program the balance between endogenous ROS generation and elimination would cause irreversible oxidative damage and eventually cell death.<sup>[11]</sup> Therefore, it is conceivable that approaches enabling to produce ROS exogenously in a controllable manner may serve as alternative strategies to photodynamic cancer therapy. For example, the Fenton reaction between catalytic transition metal ions and hydrogen peroxide ( $H_2O_2$ ) is a general source of hydroxyl radical ( $HO\cdot$ ), one of the strongest oxidants in nature. However, the reactivity of Fenton reaction relies greatly on a low pH value (that is, pH 4), which makes it difficult to be utilized in its full extent.<sup>[12]</sup> Recent studies have reported that smartly engineered nanoplatfoms allow for efficient ROS production and specific cancer therapy by integrating iron-based nanoparticles and  $H_2O_2$ , collaborating with tumor microenvironment and external stimuli.<sup>[13]</sup> Although this concept is still in its infancy, non-photodynamic systems towards tipping the balance of ROS to induce cell death while excluding the need for external inputs have shown great promise for effective cancer therapy.<sup>[14]</sup> In fact, the delicate balance of intracellular ROS level in cancer cells make these cells depend heavily on antioxidant systems and vulnerable to further oxidative stress.<sup>[11b]</sup> Based on the different redox status between normal and cancer cells, the ideas of inducing preferential cancer cell death by exogenous ROS-generating agents have gained considerable momentum.<sup>[2a,15]</sup>

Herein, we report an activatable singlet oxygen ( $^1O_2$ ) generating system for specific cancer therapy under tumor acidic pH environment through engineering the reaction between linoleic acid hydroperoxide (LAHP) and catalytic iron(II) ions. LAHP is one of the primary products of lipid

[\*] Dr. Z. Zhou,<sup>[†]</sup> R. Tian, Prof. L. Nie

State Key Laboratory of Molecular Vaccinology and Molecular Diagnostics, Center for Molecular Imaging and Translational Medicine, School of Public Health, Xiamen University  
Xiamen 361102 (China)  
E-mail: nielm@xmu.edu.cn

Dr. Z. Zhou,<sup>[†]</sup> Dr. J. Song,<sup>[†]</sup> R. Tian, Z. Yang, Dr. G. Yu, Dr. L. Lin, Dr. G. Zhang, Dr. W. Fan, Dr. F. Zhang, Dr. G. Niu, Dr. X. Chen  
Laboratory of Molecular Imaging and Nanomedicine, National Institute of Biomedical Imaging and Bioengineering, National Institutes of Health  
Bethesda, MD 20892 (USA)  
E-mail: shawn.chen@nih.gov

[†] These authors contributed equally to this work.

Supporting information and the ORCID identification number(s) for the author(s) of this article can be found under:  
<https://doi.org/10.1002/anie.201701181>.

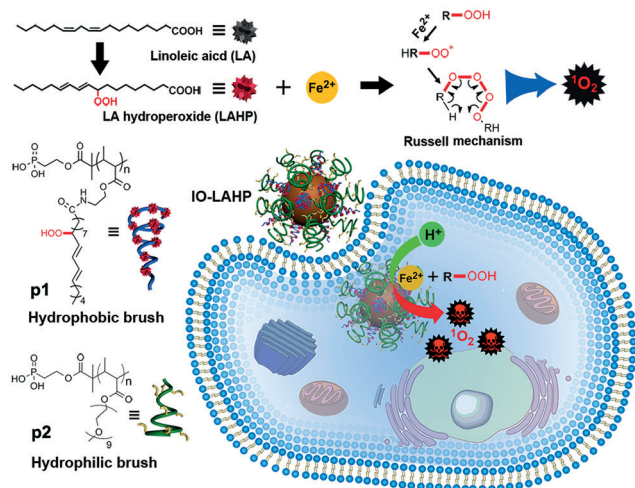


**Figure 1.** Activatable <sup>1</sup>O<sub>2</sub> generation through a biochemical reaction between LAHP and catalytic Fe<sup>2+</sup> ions by the Russell mechanism. IO-LAHP NPs were fabricated by tethering phosphate group terminated hydrophobic (p1) and hydrophilic (p2) polymer brushes on surface. After internalization with cancer cells, the release of Fe<sup>2+</sup> ions under acidic environment generate <sup>1</sup>O<sub>2</sub> species which exert cancer cell death through ROS mediated mechanism.

peroxidation, which associates with several diseases by decomposition into radicals and <sup>1</sup>O<sub>2</sub> in the presence of catalytic ions (for example, Fe<sup>2+</sup>, Ce<sup>4+</sup>) through the Russell mechanism (Figure 1).<sup>[16]</sup> Iron oxide nanoparticles (IO NPs) were employed as vehicles to carry LAHP polymers with surface-anchoring group. Hydrophilic polymers grafted with oligo ethylene glycol units were used as capping molecules on the surface of IO NPs to render the resulted IO-LAHP NPs water-dispersible, proton-penetrable, and biocompatible. It is hypothesized that H<sup>+</sup> could penetrate into the polymer brushes and dissociate Fe<sup>2+</sup> from the surface of IO-LAHP NPs, thus triggering the formation of <sup>1</sup>O<sub>2</sub> species. Upon internalization with tumor cells through endocytosis, the spontaneous generation of <sup>1</sup>O<sub>2</sub> species may result in a cascade of cancer cell death (Figure 1). The efficiency of IO-LAHP NPs for activatable <sup>1</sup>O<sub>2</sub> generation and cancer therapy were evaluated both *in vitro* and *in vivo*. Overall, we provide a novel strategy to achieve efficient cancer therapy by a non-photodynamic procedure with <sup>1</sup>O<sub>2</sub> generation from an engineered biochemical reaction.

The synthesis of LAHP was monitored by ultraviolet (UV) absorption spectrum and the reactivity of LAHP to oxidize Fe<sup>2+</sup> into Fe<sup>3+</sup> was observed (Supporting Information, Figure S1a,b). Liquid chromatography–mass spectrometry (LC-MS) was employed to further confirm the successful production of LAHP (Supporting Information, Figure S1c). A UV-based singlet oxygen scavenger 9,10-diphenylanthracene (DPA)-derived sensor and fluorescent (FL) singlet oxygen sensor green (SOSG) indicated the efficient production of <sup>1</sup>O<sub>2</sub> species by iron(II)-catalyzed decomposition of LAHP molecules, showing a significant drop in UV absorption peaks of the <sup>1</sup>O<sub>2</sub> scavenger and an increase in the FL intensity of SOSG (Figure 2 a,b). Inspired by these results, we hypothesized that IO NPs capable of on-demand release of iron(II) ions may act as a “Trojan horse” to load LAHP and

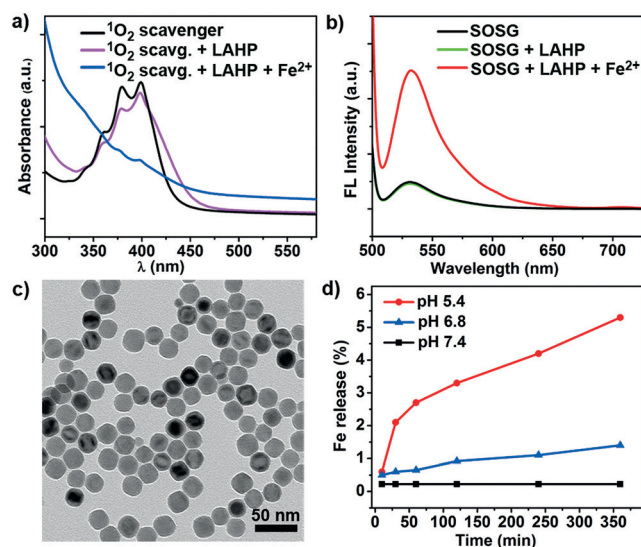


**Figure 2.** a),b) UV and FL detection of <sup>1</sup>O<sub>2</sub> generation by <sup>1</sup>O<sub>2</sub> scavenger and SOSG. c) TEM image of IO NPs of Wüstite-magnetite mixed phases with diameter of about 22 nm. d) Release profiles of iron ions from the IO-LAHP NPs under different pH values of 5.4, 6.8, and 7.4, respectively.

generate <sup>1</sup>O<sub>2</sub> species in a controllable manner. To this end, we synthesized IO NPs with metastable mixed Wüstite–magnetite (FeO–Fe<sub>3</sub>O<sub>4</sub>) phases to act as an iron(II) source to catalyze the <sup>1</sup>O<sub>2</sub> generation. Transmission electron microscopy (TEM) image showed that the as-prepared IO NPs are uniform in size with a diameter of around 22 nm (Figure 2c). X-ray diffraction (XRD) pattern, high-resolution TEM imaging, selected area electron diffraction (SAED), and fast Fourier transformation (FFT) pattern together implied typical mixed Wüstite and magnetite phases for the as-prepared IO NPs (Supporting Information, Figure S2). Magnetic hysteresis curves of the IO NPs showed partial paramagnetism with moderate saturation magnetization (*M<sub>s</sub>*) of 43.1 and 45.4 emu g<sup>−1</sup> at 300 K and 5 K, respectively (Supporting Information, Figure S3). The relatively low *M<sub>s</sub>* values for the as-prepared IO NPs could be due to the presence of antiferromagnetic Wüstite and the potential loss of long-range order of magnetic spins.

The IO NPs were then modified with polymer brushes grafted with LAHP units and terminated with a phosphate group, namely IO-LAHP NPs, assisted by hydrophilic polymer brushes grafted with oligo ethylene glycol units (Supporting Information, Figures S4 and S5). IO-LA NPs were obtained as a control. Au-LAHP NPs were fabricated as another control using similar polymers but with thiol terminal group (Supporting Information, Figures S6 and S7). TEM image and dynamic light scattering (DLS) measurement indicated good monodispersity in water with hydrodynamic diameter of about 35 nm for IO-LAHP, IO-LA, and Au-LAHP NPs (Supporting Information, Figure S8). The zeta potential of these nanoparticles showed slightly negative charges, which are probably due to the ethylene glycol groups at the outermost surface (Supporting Information, Figure S8). The hydrophilic brushes serve as capping molecules at the outer surface, which render these nano-formulations with

good biocompatibility. More importantly, the brush-like structure of hydrophilic polymers would allow for efficient water hydration, facilitating the penetration of  $H^+$  and dissolution of iron(II) ions from the surface of IO NPs in acidic environment.

Owing to the increased anaerobic glycolysis and poor perfusion under hypoxic condition, a solid tumor is overall acidic which is perhaps one of the most pervasive tumor characteristics regardless of the type.<sup>[17]</sup> Therefore, we investigated the profile of iron release from IO-LAHP NPs under different pH values (that is, 6.8 and 5.4) to mimic the tumor environment and especially endosome (or lysosome).<sup>[18]</sup> The results showed that 2.1 % of iron ions were dissolved from IO-LAHP NPs within the first 30 min incubation period which reached a value of 5.3 % after 24 h under pH 5.4 (Figure 2d). These values are 0.5 % and 1.7 % for 30 min and 24 h incubation under pH 6.8, respectively. The stability of IO-LAHP NPs against cell culture medium and fresh mouse serum were further investigated by the FL changes of SOSG. The FL of SOSG had negligible change after 24 h incubation, whereas further adding free  $Fe^{2+}$  ions into the systems led to an increase of FL intensity due to  $^1O_2$  generation (Supporting Information, Figure S9).

The feasibility of IO-LAHP NPs in upregulating intracellular ROS level was evaluated using U87MG cells as a model. First, sectional TEM images of cells after incubation with IO-LAHP NPs showed that IO-LAHP NPs entered cells mainly through endocytosis, which accumulated first in endocytic vesicles and then fused into endosomes and late lysosomes (Supporting Information, Figure S10). Furthermore, we show that both cancer U87MG and non-cancerous 293T cells uptake IO-LAHP NPs through active endocytosis which involve a combination of clathrin and caveolin mediated mechanisms (Supporting Information, Figure S11). Owing to the fact that  $^1O_2$  species are highly reactive with an extremely short half-life within tens of nanoseconds, the distance allowing for  $^1O_2$  diffusion in cytoplasm is limited.<sup>[19]</sup> However, the highly oxidative nature of  $^1O_2$  species may cause immediate oxidation of cytoplasmic substances nearby, thus elevating the intracellular ROS level. In this respect, we studied the changes of ROS level of cells treated with IO-LAHP NPs using a 2',7'-dichlorodihydrofluorescein diacetate probe ( $H_2DCFDA$ ). Confocal microscopy images and flow cytometry showed an increased level of ROS with a 3–5 fold higher median fluorescence intensity (MFI) for cells incubated with IO-LAHP NPs, compared with those incubated with PBS, IO-LA, and Au-LAHP NPs (Supporting Information, Figure S12).

We further conducted the cytotoxicity study of these nano-formulations in different cell lines. According to the thermal gravimetric analysis (TGA) and structural parameters of IO NPs (Supporting Information, Figure S13), the concentrations of LAHP molecules ( $\mu M$ ) on IO-LAHP NPs were normalized to the concentrations of iron ( $\mu g mL^{-1}$ ) by a factor of 3.54. After incubation with U87MG cells for 24 and 48 h, the  $IC_{50}$  of IO-LAHP NPs with respect to LAHP units were  $7.8 \pm 0.92$  and  $5.7 \pm 0.77 \mu M$ , which were  $27.6 \pm 3.22$  and  $20.3 \pm 2.69 \mu g mL^{-1}$  with respect to iron metals, respectively (Figure 3a; Supporting Information, Figure S14 and

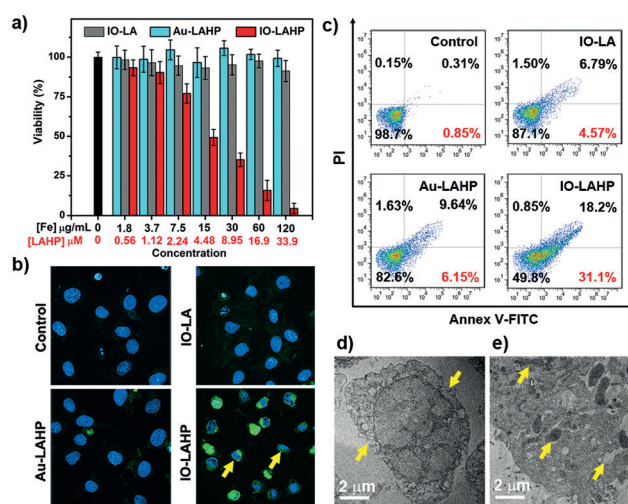


**Figure 3.** a) Cell viability study in U87MG cell model after incubation with PBS, IO-LAHP, Au-LAHP, or IO-LA NPs for 48 h. The doses of Au-LAHP NPs were normalized to LAHP molecules. Values are mean  $\pm$  s.d. ( $n=3$ ). b) Merged confocal microscopy images of cells incubated with different formulations for 24 h and stained with DAPI and TUNEL-FITC. Yellow arrows show the size shrinkage and shape abnormality of cell nucleus. c) Flow cytometry study of cells treated with different formulations for 24 h and stained with Annex V-FITC/PI apoptosis kit. Values indicate the percentages of early apoptotic cells. d, e) Sectional TEM images of cells treated with IO-LAHP NPs for 24 h, showing d) surface blebbing and membrane disruption (yellow arrows), and e) cytoplasmic vacuolation, chromatin margination, condensation, and fragmentation (yellow arrows).

Table S1). The doses of Au-LAHP NPs were normalized to LAHP molecules. Interestingly, we found that IO-LAHP NPs showed significantly greater cytotoxicity to cancer U87MG and OVCAR-8 over non-cancerous 293T cells (Supporting Information, Figure S15 and Table S1). This phenomenon is probably due to the distinctly different antioxidant responses between cancer and non-cancerous cells to oxidative stress.<sup>[20]</sup> The concept that cancer cells are more vulnerable to the increased intracellular ROS level has spurred numerous design considerations of inducing preferential cancer cell death by ROS mediated cancer treatments.<sup>[11b,15]</sup> It is hypothesized that the iron(II) activated generation of  $^1O_2$  species occurs in a full extent within a very short time-interval, which may result in an immediate increase of intracellular ROS level. We further studied the quantitative cellular uptake of IO-LAHP NPs by U87MG cells at different incubation concentrations (Supporting Information, Figure S16). Assuming that each LAHP with one hydroperoxide will produce one  $^1O_2$  molecule without bleaching, we estimated that the intracellular ROS levels are  $1.4 \pm 0.5$ ,  $3.6 \pm 0.8$ , and  $4.2 \pm 1.2 \times 10^9$  for U87MG cells incubated with 30, 60, and  $120 \mu g Fe mL^{-1}$  of IO-LAHP NPs, respectively (Supporting Information, Figure S16). These values are comparable to the reported threshold for tumor spheroids by  $^1O_2$  species (ca.  $2 \times 10^8$  molecules per cell).<sup>[21]</sup>

To investigate the mechanism of cell death by IO-LAHP NPs, we employed terminal deoxynucleotidyl transferase dUTP nick end labeling (TUNEL) method to assess the potential DNA damage after treatment. From the 4',6-

diamidino-2-phenylindole (DAPI) staining results of cells treated with IO-LAHP NPs for 24 h, we found that the cell nuclei have significantly shrunk with irregular shape compared with those treated with control samples (Figure 3b). TUNEL staining further confirmed that cells treated with IO-LAHP NPs underwent apoptosis with prominent DNA fragmentation. The loss of cell membrane integrity and the disruption of phosphatidylserine distribution on cell membrane were further revealed by Annexin V/PI co-staining and flow cytometry assay, showing 31.1% of cells in early apoptosis stage after 24 h incubation with IO-LAHP NPs, significantly higher than those of control samples (Figure 3c; Supporting Information, Figure S17). Sectional cell TEM images showed that IO-LAHP NPs caused multiple damages to cellular organelles, such as surface blebbing, membrane disruption, cytoplasmic vacuolation, and chromatin margination, condensation, and fragmentation (Figure 3d,e; Supporting Information, Figure S18). It is noteworthy that the observed cell apoptosis in our study is probably not directly induced by singlet oxygen species. Instead, the elevated ROS level may take over and trigger the cell apoptosis through the subsequent ROS-mediated mechanism.

Encouraged by the potency of IO-LAHP NPs in vitro, we further assessed their efficacy in inhibiting tumor growth in vivo. Nude mice with subcutaneous U87MG tumors were intravenously injected with different formulations (IO-LAHP, IO-LA, or Au-LAHP NPs), with PBS as a control. Owing to the different antioxidant responses between cancer and normal cells to oxidative stress, the off-target accumulation and the potential side effect of IO-LAHP NPs to normal cells could be minimized by controlling the treatment dose. The mice groups were injected with a total of three doses, each of  $3.0 \text{ mg kg}^{-1}$  of nanoparticles (metal to body weight), once daily at every three days. During this study, MR images of mouse tumors were acquired to anatomically evaluate the potential changes in tumors. As presented in Figure 4a, lesions were found in tumor of mice treated with IO-LAHP NPs (yellow arrow, dark plaque) at 6, 12, and 18 days after

the first treatment compared with those of control group. The overall tumor growth of the mouse treated with IO-LAHP NPs was significantly suppressed after the treatments (Figure 4b; Supporting Information, Figure S19). It is worth noting that mouse groups treated with IO-LA and Au-LAHP NPs also showed considerable delay of tumor growth compared with that treated with PBS, which could be due to the mild effect of iron induced pro-inflammatory macrophage polarization by IO-LA NPs and the gradual release of ROS by Au-LAHP NPs.<sup>[22]</sup> The hematoxylin and eosin (H&E) staining of tumor tissues dissected from IO-LAHP treated mice showed obviously condensed cell nucleus compared with that of control groups (Figure 4c; Supporting Information, Figure S20). We further employed TUNEL staining to confirm that tumors treated with IO-LAHP NPs underwent significantly higher level of apoptotic cancer death than those control groups (Figure 4d; Supporting Information, Figure S21). The tumor sectional TEM images further revealed chromatin condensation and fragmentation and apoptotic bodies in tumors of mice treated with IO-LAHP NPs whereas these apoptotic features were not found in the control groups (Figure 4e,f; Supporting Information, Figure S22).

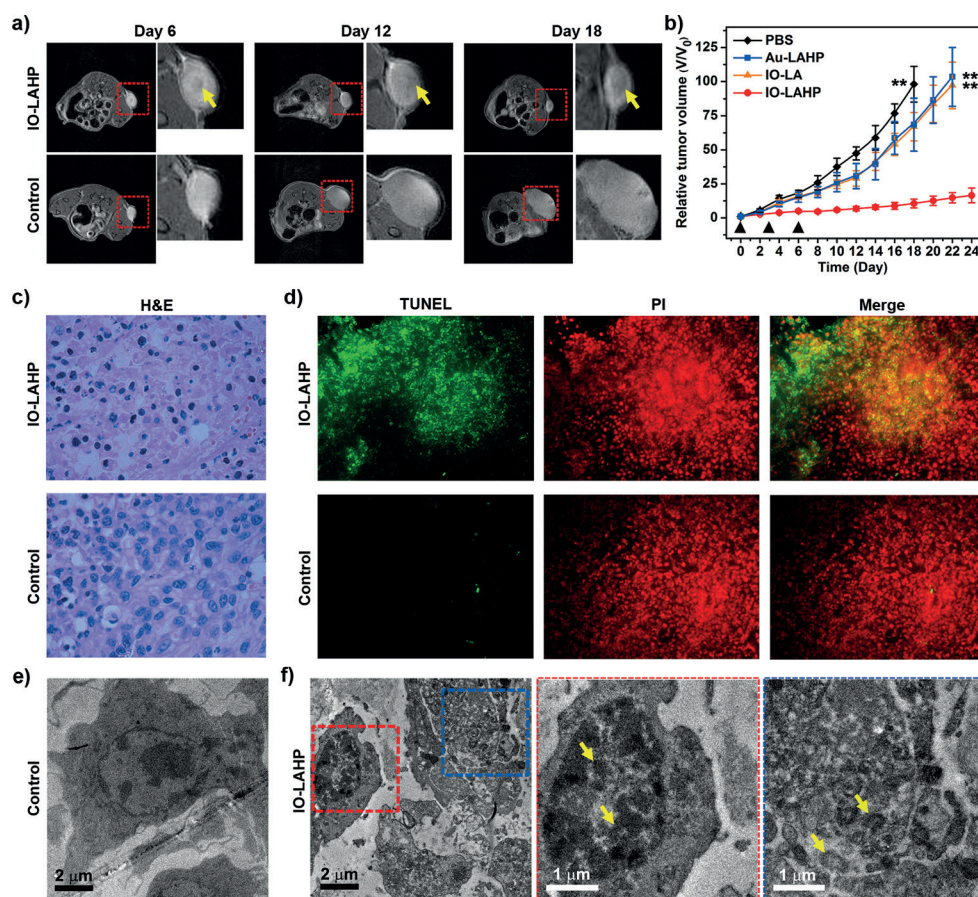


**Figure 4.** a) Typical MR images of mouse tumors after treatment with IO-LAHP or IO-LA (control) NPs through intravenous injection with a dose of  $3.0 \text{ mg kg}^{-1}$  with respect to metal mass to body weight. Images were acquired at 6, 12, and 18 days after first treatment. Yellow arrows (upper) indicate potential lesion in tumors. b) Overall tumor growth inhibition curves of mouse group treated with different formulations with total of three doses every three days (black triangles). Data represents mean  $\pm$  s.d. ( $n = 5/\text{group}$ ,  $**P < 0.01$ ). c,d) H&E and TUNEL/PI staining of tumor sections after treatment, respectively. Sectional TEM images of e) a healthy and f) a treated tumor with IO-LAHP NPs. Yellow arrows show the chromatin condensation and fragmentation (red dotted square) and the presence of apoptotic bodies (green dotted square).

In conclusion, we have developed an activatable  $^1\text{O}_2$  generation system through modulating a biochemical reaction between LAHP and catalytic iron(II) ions. The engineered IO-LAHP NPs are capable of inducing apoptotic cancer death both in vitro and in vivo through the  $^1\text{O}_2$  generation and the subsequent ROS mediated mechanism, which substantially inhibited U87MG tumor growth by intravenous administration. Importantly, the oxygen-containing LAHP molecules and the acidic-pH-induced release of iron(II) ions from IO NPs turn into the preferential  $^1\text{O}_2$  generation specifically in tumor, which kill cancers independent of oxygen or other external stimuli. Ultimately, this study potentiates the engineered biochemical reaction as a fruitful ROS resource to induce cancer cell death, which may shed light on the development of cancer treatment strategies by other biochemical reactions or substances enabling the generation of ROS.

### Acknowledgements

This work was supported by the National Science Foundation of China (81571744 and 81601489), the National Basic Research Program of China (863 Program 2015AA020502), the Fundamental Research Funds for the Central Universities (20720170065), the Science Foundation of Fujian Province (No. 2014Y2004), and by the Intramural Research Program (IRP), National Institute of Biomedical Imaging and Bioengineering (NIBIB), National Institutes of Health (NIH).

### Conflict of interest

The authors declare no conflict of interest.

**Keywords:** apoptosis · cancer therapy · iron oxide nanoparticle · lipid hydroperoxide · singlet oxygen

**How to cite:** *Angew. Chem. Int. Ed.* **2017**, *56*, 6492–6496  
*Angew. Chem.* **2017**, *129*, 6592–6596

- [1] a) R. A. Cairns, I. S. Harris, T. W. Mak, *Nat. Rev. Cancer* **2011**, *11*, 85–95; b) S. S. Sabharwal, P. T. Schumacker, *Nat. Rev. Cancer* **2014**, *14*, 709–721; c) K. Apel, H. Hirt, *Annu. Rev. Plant Biol.* **2004**, *55*, 373–399.
- [2] a) M. R. Ramsey, N. E. Sharpless, *Nat. Cell Biol.* **2006**, *8*, 1213–1215; b) A. Takahashi, N. Ohtani, K. Yamakoshi, S.-i. Iida, H. Tahara, K. Nakayama, K. I. Nakayama, T. Ide, H. Saya, E. Hara, *Nat. Cell Biol.* **2006**, *8*, 1291–1297.
- [3] a) P. Agostinis, K. Berg, K. A. Cengel, T. H. Foster, A. W. Girotti, S. O. Gollnick, S. M. Hahn, M. R. Hamblin, A. Juzeniene, D. Kessel, M. Korbelik, J. Moan, P. Mroz, D. Nowis, J. Piette, B. C. Wilson, J. Golab, *CA Cancer J. Clin.* **2011**, *61*, 250–281; b) L. Cheng, C. Wang, L. Feng, K. Yang, Z. Liu, *Chem. Rev.* **2014**, *114*, 10869–10939; c) S. S. Lucky, K. C. Soo, Y. Zhang, *Chem. Rev.* **2015**, *115*, 1990–2042.
- [4] S. B. Brown, E. A. Brown, I. Walker, *Lancet Oncol.* **2004**, *5*, 497–508.
- [5] a) W. Fan, P. Huang, X. Chen, *Chem. Soc. Rev.* **2016**, *45*, 6488–6519; b) Z. Zhou, J. Song, L. Nie, X. Chen, *Chem. Soc. Rev.* **2016**, *45*, 6597–6626; c) J. F. Lovell, T. W. B. Liu, J. Chen, G. Zheng, *Chem. Rev.* **2010**, *110*, 2839–2857.
- [6] a) H. Chen, G. D. Wang, Y.-J. Chuang, Z. Zhen, X. Chen, P. Biddinger, Z. Hao, F. Liu, B. Shen, Z. Pan, J. Xie, *Nano Lett.* **2015**, *15*, 2249–2256; b) N. Kotagiri, G. P. Sudlow, W. J. Akers, S. Achilefu, *Nat. Nanotechnol.* **2015**, *10*, 370–379.
- [7] a) H. Chen, J. Tian, W. He, Z. Guo, *J. Am. Chem. Soc.* **2015**, *137*, 1539–1547; b) C.-C. Huang, W.-T. Chia, M.-F. Chung, K.-J. Lin, C.-W. Hsiao, C. Jin, W.-H. Lim, C.-C. Chen, H.-W. Sung, *J. Am. Chem. Soc.* **2016**, *138*, 5222–5225; c) Y. Cheng, H. Cheng, C. Jiang, X. Qiu, K. Wang, W. Huan, A. Yuan, J. Wu, Y. Hu, *Nat. Commun.* **2015**, *6*, 8785; d) G. Song, C. Liang, X. Yi, Q. Zhao, L. Cheng, K. Yang, Z. Liu, *Adv. Mater.* **2016**, *28*, 2716–2723.
- [8] a) A. P. Castano, P. Mroz, M. R. Hamblin, *Nat. Rev. Cancer* **2006**, *6*, 535–545; b) D. E. J. G. J. Dolmans, D. Fukumura, R. K. Jain, *Nat. Rev. Cancer* **2003**, *3*, 380–387; c) Y. Min, J. M. Caster, M. J. Eblan, A. Z. Wang, *Chem. Rev.* **2015**, *115*, 11147–11190.
- [9] a) A. P. Wojtovich, T. H. Foster, *Redox Biol.* **2014**, *2*, 368–376; b) K. E. Mironova, G. M. Proshkina, A. V. Ryabova, O. A. Stremovskiy, S. A. Lukyanov, R. V. Petrov, S. M. Deyev, *Theranostics* **2013**, *3*, 831–840; c) P. R. Ogilby, *Chem. Soc. Rev.* **2010**, *39*, 3181–3209.
- [10] P. D. Ray, B.-W. Huang, Y. Tsuji, *Cell. Signalling* **2012**, *24*, 981–990.
- [11] a) P. T. Schumacker, *Cancer Cell* **2015**, *27*, 156–157; b) D. Trachootham, Y. Zhou, H. Zhang, Y. Demizu, Z. Chen, H. Pelicano, P. J. Chiao, G. Achanta, R. B. Arlinghaus, J. Liu, P. Huang, *Cancer Cell* **2006**, *10*, 241–252.
- [12] J. A. Lemire, J. J. Harrison, R. J. Turner, *Nat. Rev. Microbiol.* **2013**, *11*, 371–384.
- [13] a) W.-P. Li, C.-H. Su, Y.-C. Chang, Y.-J. Lin, C.-S. Yeh, *ACS Nano* **2016**, *10*, 2017–2027; b) C. Zhang, W. Bu, D. Ni, S. Zhang, Q. Li, Z. Yao, J. Zhang, H. Yao, Z. Wang, J. Shi, *Angew. Chem. Int. Ed.* **2016**, *55*, 2101–2106; *Angew. Chem.* **2016**, *128*, 2141–2146; c) H. Fan, G. Yan, Z. Zhao, X. Hu, W. Zhang, H. Liu, X. Fu, T. Fu, X.-B. Zhang, W. Tan, *Angew. Chem. Int. Ed.* **2016**, *55*, 5477–5482; *Angew. Chem.* **2016**, *128*, 5567–5572.
- [14] a) I. S. Turan, D. Yildiz, A. Turksoy, G. Gunaydin, E. U. Akkaya, *Angew. Chem. Int. Ed.* **2016**, *55*, 2875–2878; *Angew. Chem.* **2016**, *128*, 2925–2928; b) S. Kolemen, T. Ozdemir, D. Lee, G. M. Kim, T. Karatas, J. Yoon, E. U. Akkaya, *Angew. Chem. Int. Ed.* **2016**, *55*, 3606–3610; *Angew. Chem.* **2016**, *128*, 3670–3674; c) A. M. Durantini, L. E. Greene, R. Lincoln, S. R. Martínez, G. Cosa, *J. Am. Chem. Soc.* **2016**, *138*, 1215–1225.
- [15] D. Trachootham, J. Alexandre, P. Huang, *Nat. Rev. Drug Discovery* **2009**, *8*, 579–591.
- [16] a) S. Miyamoto, G. R. Martinez, M. H. G. Medeiros, P. Di Mascio, *J. Am. Chem. Soc.* **2003**, *125*, 6172–6179; b) S. Miyamoto, G. R. Martinez, D. Rettori, O. Augusto, M. H. G. Medeiros, P. Di Mascio, *Proc. Natl. Acad. Sci. USA* **2006**, *103*, 293–298.
- [17] R. A. Gatenby, R. J. Gillies, *Nat. Rev. Cancer* **2004**, *4*, 891–899.
- [18] A. Sorkin, M. von Zastrow, *Nat. Rev. Mol. Cell Biol.* **2002**, *3*, 600–614.
- [19] a) R. Li, N. D. Mansukhani, L. M. Guiney, Z. Ji, Y. Zhao, C. H. Chang, C. T. French, J. F. Miller, M. C. Hersam, A. E. Nel, T. Xia, *ACS Nano* **2016**, *10*, 10966–10980; b) T.-L. To, M. J. Fadol, X. Shu, *Nat. Commun.* **2014**, *5*, 4072.
- [20] C. Nathan, A. Cunningham-Bussel, *Nat. Rev. Immunol.* **2013**, *13*, 349–361.
- [21] S. Clement, W. Deng, E. Camilleri, B. C. Wilson, E. M. Goldys, *Sci. Rep.* **2016**, *6*, 19954.
- [22] S. Zanganeh, G. Hutter, R. Spitler, O. Lenkov, M. Mahmoudi, A. Shaw, J. S. Pajarinen, H. Nejadnik, S. Goodman, M. Moseley, L. M. Coussens, H. E. Daldrop-Link, *Nat. Nanotechnol.* **2016**, *11*, 986–994.

Manuscript received: February 2, 2017

Revised manuscript received: March 7, 2017

Version of record online: May 4, 2017